DOI: https://doi.org/10.1016/j.cattod.2020.02.029

Influence of morphology of zirconium-doped mesoporous silicas on 5-hydroxymethylfurfural production from mono-, di- and polysaccharides

S. Mérida-Morales,[a] C. García-Sancho,[a,*] M. Oregui-Bengoechea,[b] M.J. Ginés-Molina,[a] J.A. Cecilia,[a] P.L. Arias,[b] R. Moreno-Tost,[a] P. Maireles-Torres[a]

[a] *Universidad de Málaga, Departamento de Química Inorgánica, Cristalografía y Mineralogía (Unidad Asociada al ICP-CSIC), Facultad de Ciencias, Campus de Teatinos, 29071 Málaga, Spain*

[b] *Universidad del Pais Vasco - Euskal Herriko Unibertsitatea, Campus Bizkaia, Leioa, Spain*

**Corresponding author: cristinags@uma.es*

Abstract

Different zirconium-doped mesoporous silicas (Zr-KIT-6, Zr-SBA-15, Zr-MCM-41 and Zr-HMS) were synthesized and evaluated in the glucose dehydration to 5-hydroxymethylfurfural (HMF). A Si/Zr molar ratio of 5 was chosen for this purpose after the optimization of this parameter for the KIT-6 support. These materials were characterized by using XRD, N_2 sorption, TEM, XPS, NH_3-TPD and pyridine adsorption coupled to FTIR spectroscopy. All catalysts were active in glucose dehydration, being HMF the main product, and their catalytic performance is enhanced after $CaCl_2$ addition to the reaction medium. However, Zr-doped mesoporous HMS silica showed the highest values of glucose conversion and HMF yield, mainly at short reaction times, due to this catalyst displayed the highest surface zirconium concentration and its 3D morphology favored the access of glucose molecules to active sites. This fact also caused a faster deactivation due to coke deposition on the catalyst surface, although

leaching of zirconium was negligible. The Zr-HMS(5) catalyst could be reused for four catalytic runs without any treatment and the initial catalytic activity could be recovered after washing with water and acetone. This catalyst also demonstrated to be active for hydrolysis of disaccharides and polysaccharides, such as sucrose, maltose, cellobiose, inulin and cellulose, and subsequent dehydration of resulting monomers for HMF production.

Keywords: *glucose dehydration; 5-hydroxymethylfurfural, zirconium doped mesoporous silica, disaccharides, cellulose.*

1. Introduction

The pursuit of new carbon sources is becoming an essential aim owing to the decrease of fossil-fuel reserves and environmental concerns associated to their extraction, transformation and use. In this context, renewable biomass is considered a sustainable alternative, especially lignocellulose because of its abundance in nature and its chemical composition (40-50% cellulose, 25-30% hemicellulose and 15-30% lignin) [1]. Moreover, most lignocellulosic biomass does not interfere with the food chain. Cellulose and hemicellulose are mainly formed by polymerization of C6 and C5 carbohydrates, respectively, being possible their hydrolysis and transformation of the corresponding monomers to a wide variety of high value-added chemicals, such as 5-hydroxymethylfurfural (HMF) and furfural [2] through acid catalysis. As regards HMF, it is considered as an important platform molecule, from which a huge amount of valuable products can be obtained: 2,5-furandicarboxylic acid, 2,5-dimethylfuran, levulinic acid and 5-alkoxymethylfurfural, among others [3]. These compounds can be used, in turn, as building blocks for the manufacture of pharmaceuticals, polymers or

biofuels [4]. For this reason, in recent years, much attention is being paid to the production of HMF from carbohydrates.

Recent research works dealing with carbohydrate dehydration have emphasized that glucose is preferred as raw material due to its abundance and low price [3,5–7]. A route proposed for conversion of this monosaccharide to HMF consists of two steps: the isomerization of glucose to fructose and its subsequent dehydration to HMF. However, the first step is more difficult, becoming a limiting factor for an efficient HMF production. Moreover, secondary reactions, in which formic and levulinic acids as well as humins are formed [8], negatively affect to the HMF yield, so different alternatives have been proposed in order to avoid them. On the one hand, the use of an organic co-solvent allows the HMF extraction in the reaction medium, generally from the aqueous solution, reducing in this way the side reactions, being methyl isobutyl ketone (MIBK) one of most employed [9–12] because of its recommended character [13]. On the other hand, García-Sancho et al. [14] reported that an increase in both glucose conversion and HMF yield can be achieved after the addition of inorganic salts, specially $CaCl_2$. They observed that Ca^{2+} cations form complexes with two oxygen atoms of glucose, facilitating the formation of α anomer, which seems to be prone for glucose dehydration to HMF. In addition, according to Pallagi *et al.* [15], Ca^{2+} cations give rise to stronger M – OH bondings than Na^{+} ones, so it means that by using Ca^{2+} cations, the catalytic reaction would take place more efficiently than by using alkali metal cations.

In the first studies on glucose dehydration, mineral inorganic acids, such as sulfuric or hydrochloric acids, were employed as acid catalysts [1,2,16,17], because they take advantage of their low price, easy accessibility and simple applicability in the industry [4]. However, these homogeneous acid catalysts are corrosive and damaging for environment, and consequently their replacement by heterogeneous catalysts has

demonstrated to be an interesting alternative in a desirable green chemistry scenario. Moreover, solid catalysts facilitate their easy separation of the reaction medium, recovery and reuse [2]. Considering these premises, several solid acid catalysts have been previously proposed for dehydration of glucose to HMF, such as zeolites [5,6,18], and metal oxides like TiO_2, ZrO_2 or Al_2O_3 [19–23], among a plethora of acid solids.

On the other hand, mesoporous materials are being extensively employed as catalysts and supports of heteroatoms in the dehydration of different carbohydrates, such as glucose, fructose or xylose [24–27]. These solids exhibit high specific surface area, large pore size and thermal and hydrothermal stabilities, interesting features for catalysis [28–30]. Among these materials, mesoporous silicas doped with heteroatoms have been tested in the last years for dehydration of several sugars, reaching a HMF yield of 16 wt.% in the presence of mesoporous Zr-KIT-6 [7], and a 23 and 63 wt.% by using a mesoporous Zr- and Al-doped MCM-41 silica, respectively, in the presence of NaCl [27,31]. The doping of these materials with metal oxides, such as TiO_2 or ZrO_2, increases the amount of Lewis acid sites, which promote the limiting isomerization of glucose to fructose, as it has been already mentioned. Therefore, Lewis and Brönsted acid sites are required for the isomerization of glucose to fructose and the subsequent dehydration of fructose to HMF, respectively [32]. However, the textural properties and morphology of these heteroatom-doped mesoporous silicas could have a key role on the catalytic performance for HMF production. Thus, mesoporous silica with different morphologies has been proposed in the literature as support and/or catalyst. Thus, for example, MCM-41 and SBA-15 display a hexagonally packed cylindrical pores, KIT-6 exhibits Ia3d symmetry with two channel systems interconnected and HMS shows a homogeneous globular particles interconnected between them, with a size of 1 nm [25,33–35].

The aim of the present work was to study the relation between the textural and acidic properties and the catalytic behavior of different Zr-doped mesoporous silicas (Zr-KIT-6, Zr-SBA-15, Zr-MCM-41 and Zr-HMS) on the dehydration of glucose to HMF. In order to carry out the glucose dehydration, a biphasic water–MIBK solvent system was used to prevent side reactions, and the effect of $CaCl_2$ addition on the catalytic performance was also studied. Moreover, the influence of support morphology and the Si/Zr molar ratio were also evaluated, as well as different reaction parameters, such as time and temperature reaction, the amount of catalyst and, the reusability of catalysts.

2. Experimental

2.1. Materials

Zirconium-doped mesoporous silicas were synthesized using tetraethyl orthosilicate (TEOS) (98%, Aldrich) and zirconium(IV) n-propoxide (70 wt.% in 1-propanol, Aldrich) as Si and Zr sources, respectively. The structure-directing agents used for the synthesis of the different catalysts were Pluronic P123 (M_n ~ 5800 Da, Aldrich) and dodecylamine (Merck, 98%). In the catalytic test, the reagents used were D-(+)-glucose (99% GC, Sigma-Aldrich), D-(+)-Maltose monohydrate from potato (≥99%, Sigma-Aldrich), D-(+)-Cellobiose for microbiology (≥99%, Sigma-Aldrich), Sucrose BioXtra (≥99.5%, Sigma-Aldrich), Inulin from chicory (Sigma-Aldrich) and cellulose fibers (Sigma-Aldrich) as raw materials, calcium chloride dihydrate (Sigma-Aldrich) and methanol (PanReac) as well as methyl isobutyl ketone (MIBK) (GPR Rectapur, VWR) as solvents. The gases employed were N_2 (Air Liquide, 99.9999%), He (Air Liquide, 99.99%) and NH_3 (Air Liquide, 99.9%).

2.2. Catalyst preparation

A series of mesoporous Zr doped silica with a Si/Zr molar ratio of 5 was synthesized by using different methods. Likewise, the effect of the Si/Zr molar ratio was studied for mesoporous Zr-doped KIT-6. The synthetic procedures are described below. These catalysts were denoted as Zr-X(y), being X the mesostructure type and y the Si/Zr molar ratio.

2.2.1. Synthesis of Zr-KIT(y) catalysts

A series of Zr-doped mesoporous KIT-6 silicas with different Si/Zr molar ratio (Si/Zr= 5, 14 and 30) and without zirconium was synthesized. In a typical procedure [36], a solution of 5.0 g of triblock copolymer Pluronic P123 and 180 mL of 0.5 M HCl were mixed at 35ºC, under stirring, until total dissolution of P123. Then, 5.0 g of n-butanol was added, maintaining under stirring for 1 h, at the same temperature. Later, 10.6 g of TEOS and the required amount of zirconium n-propoxide were added drop by drop to the mixture and this new solution was stirred for 24 h. Finally, the mixture was transferred to an autoclave lined with Teflon and submitted to a hydrothermal treatment, and thermally treated at 100 ºC for 24 h. The solid product obtained was filtered off and washed with distilled water, dried at 65 ºC for 48 h and calcined in air at 550 ºC for 5h.

2.2.2. Synthesis of Zr-SBA(5) and Zr-SBAHT(5) catalysts

Different Zr-doped mesoporous SBA-15 silicas have been synthesized following the method proposed by García-Sancho *et al.* [37]. Firstly, P-123, used as the structure-directing agent, was dissolved in a 1.7 M HCl aqueous solution, under magnetic stirring at 40 ºC. TEOS and zirconium n-propoxide with a Si/Zr molar ratio of 5 were added dropwise. The resulting mixture was treated by two different routes: i) magnetically stirred at 40 ºC during 72 h, and ii) at room temperature for 24 h and then transferred to a teflon lined reactor and placed in an autoclave and aged at 120 ºC for 48 h. These two catalysts were denoted as Zr-SBA(5) and Zr-SBA-HT(5), respectively. In both cases,

the gel was filtered to recover the solid product and, subsequently, it was washed with deionized water, dried at 60 ºC and calcined in air at 550 ºC for 6 h, using 1 ºC·min^{-1} as heating rate.

2.2.3. Synthesis of Zr-MCM(5) catalyst

A zirconium-doped mesoporous MCM-41 silica with a Si/Zr molar ratio of 5 has been prepared by the method proposed by Jones *et al.* [38]. The synthesis was carried out by adding the corresponding amount of TEOS and zirconium n-propoxide to an ethanol-propanol solution, which was stirred for 15 min at room temperature. This solution was added to an aqueous solution of hexadecyltrimethylammonium bromide (25 wt.%), previously stirred for 30 min at 80 ºC. The pH was adjusted to 10 by using a tetramethylammonium hydroxide (25 wt.%) aqueous solution. The resulting gel was stirred for 4 days at room temperature. The solid product obtained was recovery by filtration, washed with water and ethanol, dried at 70 ºC and, finally, calcined in air at 550 ºC for 6 h using a heating rate of 1 ºC·min^{-1}.

2.2.4. Synthesis of Zr-HMS(5) catalyst

The zirconium-doped HMS silica was synthesized following the procedure proposed by Cecilia *et al.* [39]. Firstly, dodecylamine (3.1 g) was dissolved in 17.9 mL of ethanol and 21.5 mL of water. Then, a solution formed by 14.8 mL of TEOS and 5.78 mL of zirconium n-propoxide with a Si/Zr molar ratio of 5 was added dropwise to the amine solution, and the resulting solution was stirred for 24 h. Finally, the solid obtained was filtered, washed with deionized water, dried overnight at 60 ºC and calcined at 550 ºC for 6 h, with a heating rate of 1 ºC min^{-1}.

2.3. Characterization of catalysts

X-ray powder diffraction (XRPD) patterns were collected on a PANanalytical EMPYREAN automated diffractometer. Powder XRD patterns at high angle were recorded in Bragg-Brentano reflection configuration by using the PIXcel 3D detector with a step size of 0.017º (2θ), and they were recorded between 10º and 70º in 2θ with a total measuring time of 10 min. The diffractograms at low-angle were recorded in theta-theta transmission configuration, emplacing the sample between two kapton foils and by using a focusing mirror and the PIXcel 3D detector (working in 1D mode) with a step size of 0.013º (2θ), and data were recorded between 2θ = 0.5º and 10º with a total measuring time of 60 min.

Textural properties were determined by the nitrogen adsorption-desorption isotherms at -196 ºC, which were obtained from an automatic gas adsorption ASAP 2420 surface area and porosity analyzer model from Micromeritics. Before performing N_2 adsorption, samples were degassed at 200 ºC and 10^{-4} mbar for 10 h. Specific surface area values were determined by assuming a nitrogen molecule cross section of 16.2 $Å^2$ and using the Brunauer-Emmet-Teller (BET) method. Pore size distributions were calculated employing the DFT and MP methods.

X-ray photoelectron spectroscopy (XPS) studies were carried out by using a Physical Electronics PHI VersaProbe II spectrometer with non-monochromatic Al Kα radiation (53.6 W and 1486.6 eV) with a multi-channel detector. Spectra were recorded using a 200 µm diameter analysis area. Charge referencing was measured against adventitious carbon (C 1s at 284.8 eV). A PHI ACCESS ESCA-V6.0 F software package was used for acquisition and data analysis. A Shirley-type background was subtracted from the signals. Recorded spectra were always fitted using Gaussian–Lorentzian curves in order to determine accurately the binding energies of the different element core levels.

The ammonia temperature-programmed desorption (NH_3-TPD) was performed to evaluate the total acidity of catalysts. Firstly, 0.08 g of the samples were pretreated under a helium flow by heating up to 550 ºC, and, after cooling, the adsorption of ammonia was performed at 100 ºC. The NH_3-TPD was conducted by enhancing the temperature from 100 ºC to 550 ºC with a heating rate of 10 ºC min^{-1}, maintaining at this temperature for 15 minutes and using a helium flow of 40 mL min^{-1}. The evolved ammonia was analyzed by employing a TCD detector.

DRIFT spectra of adsorbed pyridine were recorded on a VERTEX 70 spectrometer coupled with an external sample chamber that enables measurements under vacuum (Bruker, Germany). The samples were mixed with KBr and grounded prior to the measurement. Samples were dried *in situ* under vacuum (around $1.5 \cdot 10^{-3}$ mbar) for 1 h at 200ºC, and later cooled down to 40ºC in order to record the background spectra. The main measurement features were a spectral range from 1800 to 1200 cm^{-1}, 200 scans, and a resolution of 2 cm^{-1}. Initially, the catalyst was put in direct contact with pyridine at 40 ºC for 8 min. Analysis were obtained by heating the samples under vacuum ($5–1 \cdot 10^{-3}$) up to 100, 125 or 175 ºC for 15 min.

Transmission electron microscopy (TEM) was used to elucidate the catalyst morphology. The equipment employed was a FEI Talos F200X combined with an outstanding high-resolution STEM, TEM imaging and an energy dispersive X-ray spectroscopy (EDS) signal detection. Moreover, a compositional mapping was done to obtain the 3D chemical characterization.

Thermogravimetric analyses (TGA) were carried out with a SDT-Q600 analyzer from TA instruments, under an air flow of 50 $mL \cdot min^{-1}$, a heating ramp of $10ºC \cdot min^{-1}$ from room temperature until 900ºC. Carbon content of fresh and spent catalysts was measured by using a LECO CHNS 932 analyzer.

2.4. Catalytic test

The glucose dehydration was carried out in batch conditions, by using a glass pressure tube with thread bushing (Ace, 15 mL) under magnetic stirring. A biphasic water-MIBK system was used with the purpose of avoiding side reactions and, consequently, enhancing the HMF yield [40]. Moreover, calcium chloride was added to the reaction medium in order to improve the HMF yield. In a typical procedure, 0.15 g of carbohydrates (glucose, disaccharides and polysaccharides in each case), 0.05 g catalyst, 0.975 g $CaCl_2$ (0.65 $g_{CaCl_2} \cdot g_{aqueous\ solution}^{-1}$.), 1.5 mL deionized water and 3.5 mL MIBK were introduced into the reactor. The catalysts were poured into reactor without previous pretreatment. Firstly, this mixture was magnetically stirred to dissolve sugar and salt and, prior to the catalytic tests, all the reactors were always purged with nitrogen. Subsequently, the catalytic process was performed in an oil bath with magnetic stirring at different temperatures. After the time established, the reaction mixture was cooled until room temperature by submerging the reactor in a cold water bath. The liquid phases were separated and filtered, and products were analyzed in both aqueous and organic phases by a High-Performance Liquid Chromatography (HPLC), being glucose, fructose and HMF the unique detected products. A JASCO instrument equipped with an autosampler (AS-2055), a quaternary gradient pump (PU-2089), multiwavelength detector (MD-2015) and a column oven (co-2065), was employed. Columns used were a Phenomenex Rezex ROA-Organic Acid H^+ (8%) (300 mm x 7.8 mm, 5 μm) for the aqueous phase, which mobile phase consisted in an aqueous dissolution 0.005 N H_2SO_4 with a flow rate of 0.35 $mL \cdot min^{-1}$ (column temperature of 40ºC), and a Phenomenex Luna C18 reversed-phase column (250 mm x 4.6 mm, 5 μm) for the organic phase, which mobile phase consisted in pure methanol with a flow rate of 0.5 $mL \cdot min^{-1}$ (room temperature). Both glucose and fructose were monitored

employing a refractive index detector only for aqueous phase, whereas HMF production was monitored by a UV detector in both phases.

The reuse experiments were performed after 60 min of reaction time at 150 ºC, by using the experimental conditions previously indicated. After each catalytic cycle, the catalyst was recovered by filtration and used without any treatment in the next cycle, whereas liquid phases were analyzed by HPLC. After the sixth cycle, the catalyst was washed with 50 mL of water and 50 mL of acetone to realize another cycle and evaluate the influence of washing on the humins removal and HMF yield as well.

The glucose conversion, HMF selectivity and yield were calculated applying the following equations:

$$\text{glucose conversion (\%)} = \frac{\mu\text{moles of initial glucose} - \mu\text{moles of final glucose}}{\mu\text{moles of initial glucose}} \text{ x } 100 \qquad (1)$$

$$\text{HMF selectivity (\%)} = \frac{\mu\text{moles of HMF obtained}_{aq} + \mu\text{moles of HMF obtained}_{org}}{\mu\text{moles of initial glucose} - \mu\text{moles of final glucose}} \text{x } 100 \qquad (2)$$

$$\text{HMF yield (\%)} = \frac{\text{glucose conversion x HMF selectivity}}{100} \qquad (3)$$

Finally, different disaccharides and polysaccharides were evaluated as feedstocks for HMF production. The procedure was the same as described above for the glucose dehydration. The reaction conditions were T= 175ºC, t= 60 min, 0.65 $g_{CaCl2} \cdot g_{aqueous\ solution}^{-1}$, MIBK:water (v/v)= 3.5:1.5 and sugar:water weight ratio= 1:10. Sugars employed were sucrose, maltose, inulin, cellobiose and cellulose, and the chosen proved was the Zr-HMS (5). HMF yield was calculated as follows:

$$HMF\ yield\ (\%)$$

$$= \frac{grams\ of\ HMF\ obtained_{aq} + \ grams\ of\ HMF\ obtained_{org}}{grams\ of\ initial\ disaccharide\ or\ polisaccharide}\ x\ 100 \quad (4)$$

3. Results and discussion

3.1. Characterization of catalysts

All catalysts were characterized by X-ray diffraction (XRD) to confirm their mesostructured nature. In the case of Zr-KIT(y) samples with different Si/Zr molar ratio (Fig. 1A), a peak located between 0.79-0.90° can be observed in the low-angle region, corresponding to (211) planes in a cubic Ia3d symmetry [41]. The KIT morphology consists of a 3D cubic network with long range order and interconnectivity between pores [36]. In addition, the X-ray diffraction patterns of KIT and Zr-KIT(30) show the characteristic (220) reflection between 1-2°, which is indicative of a well ordered mesoporous structure [36–44]. However, the intensity of these peaks decreases with the amount of Zr, that is, for lower Si/Zr molar ratio, which suggests that a high percentage of zirconium can adversely affect the KIT-6 framework, mainly for Zr-KIT(5). Thus, the Zr addition seems to influence the silica polymerization, resulting in less ordered structures. In this sense, the XRD patterns of the rest of mesoporous silicas with a Si/Zr molar ratio of 5 corroborate the negative effect of Zr incorporation on the long-range order of mesoporous framework (Fig. 1S). On the other hand, the typical broad band associated to the amorphous silica walls can be seen in the high angle region (not shown). However, the characteristic reflections of crystalline ZrO_2 were not detected, thus meaning that Zr species are homogenously dispersed into the siliceous framework or are too small to be detected by XRD.

This fact has been corroborated by Transmission Electron Microscopy (TEM) coupled to EDX analysis, which have demonstrated that zirconium species were homogenously

dispersed in the mesoporous structure (Fig. 2). Moreover, it is noticeable the lack of long-range order of catalysts with a Si/Zr molar ratio of 5, as was deduced from XRD data.

On the other hand, textural properties of catalysts were determined from their N_2 adsorption-desorption isotherms at -196 ºC (Table 1). All Zr-KIT(y) catalysts display a Type IV isotherm (Fig. 3A), characteristic of mesoporous materials [45]. Moreover, the hysteresis loops of Type H1 is typical of mesoporous solids and specially of templated silicas, as observed for KIT-6, Zr-KIT(30) and Zr-KIT(14) materials, and reveals that these catalysts possess ordered and controlled pores. However, Zr-KIT(5) displays a hysteresis loop of Type H2, which can be associated with pore blocking [45], caused for the incorporation of a high amount of zirconium into the framework. Regarding other Zr-doped mesoporous silicas studied in this work, they exhibited Type IV isotherms (Fig. 3B). In the case of Zr-doped SBA-15 catalysts, mainly for Zr-SBA-HT(5), the hysteresis loop is shifted to higher values of relative pressures, indicating the formation of wider pores. The Zr-SBA(5) catalyst showed a hysteresis loop Type H2a, whereas Zr-SBA-HT(5) is between Types H2a and H2b, which is typical of less ordered macroporous solids and it has been found for certain mesoporous ordered silicas after hydrothermal treatment [45]. With respect to pore size distributions determined by DFT method, all materials exhibit pore sizes centered in the range of mesopores (Figs. 4A and 4B). In particular, the pore size decreases after the Zr incorporation for Zr-KIT(y) catalysts, mainly for the catalyst with the highest Zr concentration (Fig. 4A), which confirms that the presence of a high amount of Zr affects to the textural properties of mesoporous silica. It should be noticeable that values of BET surface and pore volume decrease with the Zr loading, which agrees with previous conclusion about the pore blocking. In any case, high values of surface area (462-909 m^2g^{-1}) and pore volume

(0.413-1.328 cm^3g^{-1}) were found for all Zr-doped mesoporous silica catalysts, although they differ depending on their structure and morphology. With respect to Zr-doped mesoporous SBA-15 catalysts, Zr-SBA-HT(5) exhibits higher pore size than Zr-SBA(5), since hydrothermal conditions favor an increase in pore size (Fig. 4B). As smaller pores (< 2 nm) were detected by DFT for all catalysts (Figs. 4A and 4B), they were evaluated by the MP method, which is more suitable for pores between 0.4815 and 1.920 nm hydraulic radius, including wide micropores and narrow mesopores. It can be observed that high values of surface area and pore volume were found by this method in all cases, especially for Zr-KIT(y) catalysts (Table 1). Indeed, in the case of this family of materials, pore size distribution determined by MP-method revealed the presence of uniform pore size between 1.5-2.2 nm (Fig. 4C), demonstrating the presence of wide micropores for these materials. Similar pore sizes were found for Zr-SBA(5) catalyst, but these micropores were not detected for Zr-SBAHT(5) due to hydrothermal conditions employed for its synthesis, as it has been mentioned (Fig. 4D). Indeed, the Zr-SBA-HT(5) catalyst displayed a very low microporosity due to the use of hydrothermal conditions for its synthesis provoked that the distance between micelles was bigger, in such a way that the microporosity between channels was lost after calcination [46]. In the cases of Zr-MCM(5) and Zr-HMS(5) catalysts, lower pore size than 1.5 nm were found for this method. Therefore, pore size distribution was not homogeneous in any case, since different pore sizes were detected for these materials by DFT and MP methods.

Acid properties were evaluated by ammonia temperature-programmed desorption and adsorption of pyridine coupled to FTIR spectroscopy. The first technique was used to ascertain the total acidity (Table 1), while the second one was used to analyze Brönsted and Lewis acid sites. All catalysts showed a high total acidity,

especially Zr-KIT catalysts, and the total acidity enhances with the increase in the zirconium amount incorporated to the framework. Thus, it is confirmed that the presence of this heteroatom rises the acidity of these solids. The highest values of acid density are for KIT-6 and hydrothermal SBA-15 materials (Table 1). Comparing for the same Si/Zr molar ratio, the Zr-HMS(5) and Zr-MCM(5) catalysts displayed the lowest values of total acidity and acid density. This fact could be related to their different synthesis conditions, since both catalysts were prepared in basic conditions, whereas the rest of catalysts (Zr-KIT(5), Zr-SBA(5) and Zr-SBA-HT(5)) were in acid medium. Therefore, it could be thought that acid or basic synthesis conditions influence on the hydrolysis rate, modifying the Zr environment into the siliceous framework and subsequently their acidic properties. Thus, the faster hydrolysis rate in basic medium would lead to a higher amount of Zr was located inside the walls of the siliceous framework, not accessible for NH_3 molecules. On the other hand, FTIR spectra after pyridine adsorption exhibit an IR vibrational band at 1445 cm^{-1}, even after evacuating at temperatures as high as 150 and 175 ºC, which is assigned to the 19b vibration mode of pyridine coordinated to strong Lewis acid sites (Fig. 5) [44]. Moreover, the band centered at 1596 cm^{-1} is observed for all catalysts, and it can be attributed to the 8a vibration mode of pyridine bonded by hydrogen bond to the hydroxyl groups of the catalyst surface [47,48]. Likewise, a shoulder about 1578 cm^{-1} can be seen mainly for Zr-MCM(5) and Zr-SBA(5) catalysts, after evacuation at lower temperature (100 ºC), which is attributed to pyridine coordinated on weak Lewis acid sites [49]. However, this band disappeared when the evacuation temperature increased, thus corroborating the weakness of these Lewis acid sites. Another shoulder can be detected at 1613 cm^{-1} for Zr-KIT(5), Zr-SBA(5) and Zr-HMS(5) catalysts, which is also associated to the 8a vibration mode of pyridine coordinated to strong Lewis acid sites. However, it can be

noticeable the absence of the characteristic band at 1540 cm^{-1} attributed to pyridine adsorbed on Brönsted acid sites. However, the formation of Brönsted acid sites in the reaction medium cannot be discarded due to Lewis acid sites could be transformed to Brönsted ones in the presence of water at high temperature [26,50]. With respect to the strength of acid sites, the most intense bands detected at 1445 and 1596 cm^{-1} were still observed after outgassing at 150 and 175 ºC, demonstrating their strong acid strength, although their intensity decreased with respect to those obtained after outgassing at 100ºC, as expected.

XPS analysis was employed to get insights into the nature of catalyst surface (Table 2). The values of binding energies (BE) provide useful information about the environment of surface chemical elements. The Si 2p signal appeared at 103.1-103.8 eV, which is typical of Si in silica. On the other hand, the incorporation of Zr species into the siliceous framework was confirmed by the binding energies for Zr $3d_{5/2}$, which were in the range of 182.8-183.4 eV, attributed to Si-O-Zr bonds in the literature [51,52]. These BE values are higher than that of bulk ZrO_2 (182.2 eV) [53,54], so the existence of segregated ZrO_2 could be discarded, according to the data obtained by XRD. In the O 1s spectral region, the catalysts with lower Zr concentration (Zr-KIT(30) and Zr-KIT(14)), showed a symmetric band centered at 532.4-532.7 eV. However, this band became asymmetric when the amount of Zr was increased, and it could be deconvoluted into two components located at 530.7-530.8 eV and 532.4-533.0 eV. The former was considerably less intense in all cases, finding the highest contribution (7.8%) for Zr-HMS(5), and can be attributed to Si-O-Zr which would confirm the replacement of Si by Zr atoms [33,44]. Moreover, this BE is higher than that found for bulk ZrO_2 (529.9–530.2 eV) [55]. The latter (532.4-533.0 eV) was considerably more intense and is characteristic of Si-O-Si bonds in silica [44]. It should also be noted that

the BE of O 1s associated to Si-O-Si bonds of Zr-KIT(y) catalysts slightly increased after incorporation of a high amount of zirconium, whereas values of BE for Si 2p decreased. This fact could be due to the presence of zirconium decreased electronic density of oxygen and increased for silicon, demonstrating the incorporation of Zr to the siliceous framework. As regards the surface Si/Zr molar ratio determined by XPS, in all cases, they are higher than the nominal ones, except for the Zr-KIT(30) catalyst where the low loading of Zr could allow a homogeneous dispersion in the siliceous matrix. When the catalysts with the same Si/Zr molar ratio were compared, both Zr-SBA(5) and Zr-SBA-HT(5) exhibited the highest surface Si/Zr molar ratio, which could be explained by their thick mesoporous walls in comparison to the other mesoporous framework (MCM-41, HMS and KIT), where Zr can be encapsulated limiting the amount of Zr detected by XPS. It must be taken into account that the thickness of the outer surface analyzed by this technique is around 2-3 nm. However, Zr-MCM(5) and mainly Zr-HMS(5) provided the lowest Si/Zr molar ratio, which could be ascribed to the basic conditions used for their synthesis and the low thickness of their walls. In any case, the higher surface Si/Zr molar ratios, compared with the values used in the synthesis (labelled as bulk in Table 2), can be justified by the higher hydrolysis rate of zirconium precursor, which provokes a progressive impoverishment in zirconium when going from internal to external regions of mesoporous solids.

3.2. Catalytic tests

These Zr-doped mesoporous silicas have been tested as heterogeneous acid catalyst for the glucose dehydration to HMF. Because of the instability of this product in water, a biphasic system is often used to extract HMF from the aqueous phase and, therefore, to minimize side reactions such as resinification and condensation reactions, which are involved in humins formation, whom decrease the HMF yield as well [56].

Organic co-solvents have demonstrated to be an interesting option for this purpose, being methyl isobutyl ketone one of the most reported in the literature with better results in terms of HMF yield [14,27,44].

In a previous work, it was demonstrated that the presence of $CaCl_2$ considerably enhances the catalytic activity of γ-Al_2O_3 for dehydration of glucose to HMF, due to Ca^{2+} ions favor the α-D-glucopyranose formation [14]. Thus, firstly, the effect of $CaCl_2$ addition in the reaction medium was evaluated at 175 ºC, by using Zr-KIT(14) as catalyst (Fig. 6A). It can be observed that glucose conversion and HMF yield are improved after incorporation of $CaCl_2$ to the reaction medium. This positive effect was explained to the facility of alkaline earth metal cations to form bidentate complexes by their interaction with two oxygen atoms of glucose [57]. In this sense, García-Sancho *et al.* demonstrated that $CaCl_2$ exerted a positive influence greater than NaCl, respect to the study in the absence of inorganic salts [14]. Therefore, the rest of catalytic tests were carried out in the presence of calcium chloride in order to maximize the HMF production.

On the other hand, the influence of Si/Zr molar ratio for Zr-KIT(y) catalysts on the catalytic performance was also evaluated at 175 ºC (Fig. 6B). Although drastic differences were not detected, Zr-KIT(5) was the most active catalyst, attaining a higher glucose conversion, mainly at shorter reaction times. Regarding HMF yield, this catalyst provided the maximum value after only 60 minutes, and then it decreased progressively due to the side reactions consuming HMF. Thus, the highest glucose conversion and HMF yield were obtained for the Zr-KIT(5) catalyst, achieving values of 88% and 45%, respectively, after 60 minutes of reaction. Moreover, the results obtained in the present study are better than those reported by Chongwen *et al.* [7] by using a Zr-doped mesoporous KIT-6 with a Si/Zr molar ratio of 20 as catalyst, since,

after 3 h at 170ºC, with a MIBK/water ratio of 4, a glucose conversion of 79% and HMF yield of 34.5%, were only reached. This better catalytic performance was possibly due to the combined use of a higher Zr concentration and the addition of $CaCl_2$. In any case, a glucose conversion and HMF yield of 36 and 7%, respectively, were achieved with Zr-KIT(14), without the addition of $CaCl_2$ after 60 min at 175ºC (Fig. 6A), whereas Chongwen *et al.* obtained less than 30% of glucose conversion and less than 4% of HMF yield at the same time and similar temperature [7].

Secondly, the catalytic behavior of Zr-KIT(5) was compared with other mesostructured silicas with a similar Si/Zr molar ratio, but different framework type (Zr-HMS(5), Zr-SBA(5), Zr-SBA-HT(5) and Zr-MCM(5)), at 175 ºC, in the presence of $CaCl_2$ (Fig. 7). In all cases, the glucose conversion enhanced with the reaction time, attaining full glucose conversion after 120 min in the presence of Zr-HMS(5), unlike the rest of catalysts, with maximum values of 88 and 91% for Zr-MCM(5) and Zr-KIT(5), after 120 min, respectively, and close to 80% for Zr-SBA(5) and Zr-SBA-HT(5), after 90 min. The lowest values of glucose conversion were found for Zr-doped mesoporous SBA-15 silicas, which showed the highest surface Si/Zr molar ratio and consequently the lower concentration of surface Zr species. Moreover, the adsorption study of pyridine coupled to FTIR spectroscopy demonstrated the absence of strong Lewis acid sites in SBA-15-based catalysts, which would difficult glucose dehydration in comparison with the rest of catalyst. In the case of the most active catalyst, Zr-HMS(5), the lowest surface Si/Zr molar ratio was found, that is, its surface is richer in Zr species. Thus, Fig. 8 shows that there is a trend for surface Si/Zr molar ratio lower than 15, in such a way that the catalytic activity was higher when this surface ratio decreased. However, it did not decrease, as it was expected, for surface Si/Zr molar ratio higher than 15, obtaining similar catalytic data for Zr-SBA(5) and Zr-SBA-HT(5) than Zr-

MCM(5) in spite of the important differences in their surface Zr concentration. This fact could be due to these materials possess a hexagonally packed cylindrical pores unlike Zr-HMS(5) and Zr-KIT(5) catalysts. Therefore, it could be concluded that the surface Zr concentration and morphology of catalysts play a key role for HMF production by glucose dehydration, mainly at shorter reaction times when the degradation processes are still incipient. It is obvious that most acid sites are associated to Zr centers, and a high surface Zr concentration favors the interaction with glucose molecules, in such a way that the HMF production takes place more quickly. Considering that the same alkoxides were employed in all synthetic routes, different surfactants and conditions must be responsible of the different surface Zr contents, probably due to different hydrolysis rates, faster in the case of Zr species and even more in basic medium, according to XPS data previously discussed. However, the best catalytic performance of Zr-KIT (5) compared to Zr-MCM (5), both synthesized in acidic conditions, could be associated with its much higher specific surface area (701 *versus* 564 $m^2\ g^{-1}$). Therefore, it could exist a relation between the surface Si/Zr molar ratio and surface area. Thus, values of glucose conversion after 20 min of reaction were represented as a function of surface Zr atoms·nm^{-2}, considering BET surface area values (Fig. 8B). It can be observed that catalytic activity enhances with the surface Zr atoms·nm^{-2}, attaining the maximum value for Zr-HMS(5) with 0.236 at. Zr·nm^{-2}. Nevertheless, worst catalytic data were attained for Zr-MCM(5), which exhibits the highest surface Zr atoms·nm^{-2} value. This fact could be due to this catalyst possesses a hexagonally packed cylindrical pores that would difficult the access of glucose molecules to its active sites. Therefore, it seems that the Zr-HMS(5) catalyst possesses the best combination between textural parameters and surface Zr concentration to maximize dehydration of glucose to HMF. From these data, it can be supposed that the 3D structure of Zr-KIT(5) and, mainly, the

globular structure of Zr-HMS(5) would facilitate the access of glucose molecules to surface zirconium sites.

Regarding the HMF yield, similar trends to those observed for glucose conversion were found in all cases. However, it must be taken into account the existence of side reactions that decrease the HMF yield for longer reaction times, when condensation and resinification reactions between HMF, glucose and intermediates are more likely to occur [58]. In addition, low fructose yields were observed in all cases owing to its fast transformation into HMF, thus confirming that isomerization of glucose to fructose is the limiting step of HMF production from glucose and the Lewis acidity provided by the zirconium supported on mesoporous silica has been effective to catalyze this process, as well as the $CaCl_2$ presence helps with this aim.

On the other hand, the interconnection between pores of HMS would allow HMF molecules faster leave pores, increasing the HMF production at shorter reaction times, as can be inferred from Fig. 7. However, this catalyst showed an important fraction of micropores with sizes lower than 1.2 nm, which would provoke its faster deactivation because of the pore blocking and diffusional limitation of reactant and products. In this sense, for reaction times longer than 60 min, the HMF yield started to decrease more quickly than with the other Zr-doped mesoporous silicas, which could be due to deactivation of active sites or the leaching of Zr species. For this reason, ICP-MS was used to evaluated the presence of soluble Zr species in the reaction medium after a catalytic test carried out at 175 ºC after 90 min, with the aim to verify if it was the cause of the Zr-HMS(5) deactivation, but this analysis showed an insignificant Zr presence (0.06%). Therefore, it could be supposed that deactivation was due to the deposition of organic species on active sites. To verify this assumption, the used catalyst was recovered and CHN analysis has corroborated the existence of these species, since the C

content increased from 0.08 wt.% for the fresh catalyst until 5.92 wt.% for the spent one. Indeed, the surface C atomic concentration of spent Zr-HMS(5) catalyst, determined by XPS, was 67.5%, which would explain its deactivation. Likewise, the TG analysis of the spent Zr-HMS(5) catalyst reveals a weight loss of 63.65 wt.%, quite higher than that observed for the fresh Zr-HMS(5) (29.33 wt.%) (Fig. 9). This fact would point to the humins formation during the catalytic reaction as responsible the catalyst deactivation.

Due to its high catalytic performance, the following studies have been focused on the Zr-HMS(5) catalyst. Moreover, dehydration of glucose to HMF using catalysts based on MCM-41, SBA-15 and KIT-6 has been already reported in the literature [7,25,27], but with lower HMF yield than the achieved in the present work. For example, Jiménez-Morales *et al.* reached a HMF yield lower than 10% after 60 minutes and 175ºC, by using ta Zr-doped mesoporous MCM-41, whereas, under similar experimental conditions in the present work, the HMF yield obtained with the Zr-MCM(5) was 38%. Zhang *et al.*, with a sulfated zirconia SBA-15 catalyst, achieved a HMF yield of 27%, after 60 min at 140ºC, being lower than that achieved for Zr-SBA(5) (32%), after 60 min and 175ºC, in spite of the sulfated groups. However, it is the first time to the best of our knowledge that Zr-doped HMS silica is employed as catalyst for this reaction.

Likewise, a catalytic test by using the Zr-HMS(5) impregnated with pyridine (pyr-Zr-HMS(5)) as catalyst was performed to complete the influence of acidity on the catalytic performance. For this, a beaker with 3 mL of pyridine and another one with the appropriate amount of catalyst were introduced in a desiccator for 72 h. Then, the catalyst impregnated with pyridine vapors was evaluated in glucose dehydration, under similar experimental conditions. The catalytic performance of pyr-Zr-HMS(5) revealed

that both the glucose conversion and the fructose selectivity were higher after impregnation with pyridine, but the HMF yield was lower (Fig. 10). These results demonstrate that, although Lewis acid sites were blocked by pyridine, the presence of this base in the reaction medium would favor the isomerization step, since it is also catalyzed by basic sites. Thus, glucose conversion and fructose selectivity were enhanced. However, it can be noticeable that the HMF selectivity was lower in the presence of pyr-Zr-HMS(5), because a fraction of Lewis acid sites were blocked by pyridine and the basic medium provided by the pyridine did not facilitate the dehydration step of fructose to HMF, which requires the presence of acid sites.

In order to decrease the side reactions which provoke the deactivation of Zr-HMS(5), the reaction temperature was decreased at 150ºC (Fig. 11). As it was expected, glucose conversion data were lower than those attained at 175ºC, in such a way that the maximum conversion (79%) was reached after 180 min. Moreover, the fructose yield was higher at lower reaction temperature, but decreased with the reaction time, whereas concomitantly the HMF yield raises, thus supporting the two-step mechanism of glucose dehydration: isomerization of glucose to fructose and subsequent dehydration of fructose to HMF. However, the decrease in HMF yield was not observed at 150ºC, attaining a maximum value (40%) similar to that reached at 175ºC, but at longer reaction times (180 min *versus* 40 min). It should be noted that the use combined of Zr-HMS(5) and $CaCl_2$ provided higher values of glucose conversion and HMF yield that if only $CaCl_2$ was employed. By considering the catalytic behavior of Zr-HMS(5), the evaluation of the influence of other reaction parameters has been carried out at 150ºC to minimize secondary reactions, which decrease the HMF production.

The next step in the catalytic study was to evaluate the influence of the glucose:catalyst weight ratio on the catalytic performance, modifying the amount of

catalyst employed. In previous works, it was found an optimal ratio of 3 for the glucose conversion into HMF by using H-ZSM-5 zeolites as catalysts [59]. However, it is important to optimize this parameter for Zr-HMS(5). In this sense, the glucose:catalyst weight ratio was varied between 10:1 to 1:1, at 150ºC after 3 h, keeping in mind the best results attained under similar experimental conditions (79% of glucose conversion and 39% of HMF yield) (Fig. 12A). The glucose conversion enhanced with the glucose:catalyst weight ratio, reaching a maximum conversion value of 92% for a glucose:Zr-HMS(5) ratio of 1:1. The HMF yield also increased with the glucose:catalyst weight ratio, but the values attained by using 3:1 and 1:1 ratio were quite similar (39% and 41%, respectively) in spite of glucose conversion was higher for the last ratio. This means that selectivity is better for the 3:1 ratio, which could be explained by the increase in the glucose conversion by using a 1:1 ratio, the HMF production also enhanced, but this excess of HMF would favor side reactions, thus decreasing the HMF yield. This enhancement of side reactions with the amount of catalyst employed was also corroborated in Figure 12 B. Thus, the use of higher catalyst concentrations led to productivity of glucose dehydration, expressed as $g_{glucose\ converted} \cdot g_{cat}^{-1}$ and g_{HMF} formed $\cdot g_{cat}^{-1}$, was lower. This fact was probably due to a higher amount of catalyst favored the formation of secondary products.

An important advantage of heterogeneous catalysts is their reuse, and for this reason this catalyst was studied during seven catalytic cycles at 150 ºC for 60 min, under similar experimental conditions. In this case, the glucose:catalyst weight ratio used was 1:1, because a higher amount of Zr-HMS(5) in the reaction medium was easier to recover in order to carry out the subsequent cycle, without losses of catalyst. It can be observed (Fig. 13) that the glucose conversion barely changes along the different cycles. However, the HMF yield was maintained along four catalytic runs, but it started to

decrease from the fifth one. It should be noted that a slightly higher HMF yield was found in the second cycle. This fact could be explained because of the existence of HMF adsorbed on the catalyst after the first cycle, so the desorption of these HMF molecules could take place in the next cycle, consequently increasing the HMF yield. In order to corroborate this fact, the catalyst after the first catalytic cycle was washed with water and MIBK to desorb HMF molecules and the resulting solutions were analyzed by HPLC to prove qualitatively this desorption of HMF. In both cases, the presence of HMF was detected in the corresponding chromatograms (not shown), so it could be concluded that the increase in HMF yield after the first cycles was due to desorption of HMF molecules formed during the first catalytic run. On the other hand, the HMF yield maintained a progressive decay, more important after four cycles, due to catalyst deactivation associated to the deposition of humins, which adversely affect to the catalytic performance [60]. In order to recover the catalytic activity of Zr-HMS(5), the catalyst was washed with water and acetone after the 6^{th} cycle (noted as * in Fig. 13). Thus, the HMF yield in the seventh cycle enhanced with respect to the sixth one due to the removal of soluble humins by washing, attaining a value similar to the first catalytic cycle. Moreover, the TG analysis of the spent catalyst showed a weight loss of 56.39 wt.%, lower than that observed after reaction at 175 ºC since the side reactions decreased, but it was higher than the value obtained for fresh catalyst (Fig. 9). Therefore, it is demonstrated that washing was effective to remove adsorbed organic species, including HMF, since the weight loss of spent catalyst after washing were near to that of the fresh one, being even lower in the case of washing with water and ketone, demonstrating its efficiency. As a result of these tests, it can be concluded that Zr-HMS(5) can be reused for four cycles, maintaining a similar HMF yield, being even able to perform some more after washing it with water and an organic solvent.

Finally, the catalytic behavior of Zr-HMS(5) for HMF production was also studied by using different disaccharides and polysaccharides (Fig. 14). These reactions were carried out at 175 ºC because the hydrolysis reaction of disaccharides or polysaccharides was also required. It can be observed that the Zr-HMS(5) catalyst was active in both hydrolysis and dehydration processes. With respect to disaccharides, values of HMF yields equal to 24%, 27% and 33% were attained for sucrose, maltose and cellobiose, respectively. It is noteworthy to mention that higher values were achieved with maltose and cellobiose, formed by two glucose monomers, which demonstrates that the Zr-HMS(5) catalyst is able to carry out efficiently dehydration of glucose, since it was even higher than that obtained for sucrose which is formed by glucose and fructose. On the other hand, this catalyst was active for hydrolysis of polysaccharides and subsequent dehydration of resulting monomers, attaining HMF yields of 29% and 9% by using inulin and cellulose, respectively, under these reaction conditions. Therefore, the Zr-HMS(5) catalyst possesses great potential to be used as acid catalyst for HMF production from lignocellulosic biomass.

Conclusion

Zirconium-doped mesoporous silicas with a Si/Zr molar ratio of 5 have demonstrated to be active in the glucose dehydration to HMF, obtaining a more efficient catalytic performance after $CaCl_2$ addition. Although the presence of acid sites is required for glucose dehydration into HMF, a clear correlation between acidity and catalytic performance was not observed. The present work has shown that textural properties and morphology also play a key role in catalytic behavior. Thus, MCM-41 and SBA-15 morphologies, consisting of hexagonally packed cylindrical pores, are less active due to both the steric hindrance which limits the access of glucose molecules to active sites inside channels and their lower surface Zr concentration. However, the 3D

structure of Zr-KIT(5) and, mainly, the globular structure of Zr-HMS(5) facilitate the access to surface zirconium sites, in addition to presenting a high surface area and surface enrichment of Zr, as inferred from N_2 sorption and XPS analysis, respectively. Moreover, Zr-HMS(5) can be reused for four catalytic runs without any treatment between cycles, and recovering its initial catalytic activity after washing with water and acetone to remove carbonaceous species deposited on the catalytic surface. The Zr-HMS(5) catalyst was also active for hydrolysis and subsequent dehydration of disaccharides and polysaccharides, achieving similar values of HMF yield than those observed by using glucose.

Acknowledgements

The authors are grateful to financial support from the Spanish Ministry of Economy and Competitiveness (RTI2018-94918-B-C43 and C44 projects), Junta de Andalucía (RNM-1565), FEDER (European Union) funds (UMA18-FEDERJA-171) and Malaga University. C.G.S. also acknowledges FEDER funds for financial support.

References

[1] P. Zhou, Z. Zhang, Catal. Sci. Technol. 6 (2016) 3694–3712.

[2] M.A. Kougioumtzis, A. Marianou, K. Atsonios, C. Michailof, N. Nikolopoulos, N. Koukouzas, K. Triantafyllidis, A. Lappas, E. Kakaras, Waste and Biomass Valorization. 9 (2018) 2433–2445.

[3] Z. Xue, M.G. Ma, Z. Li, T. Mu, RSC Adv. 6 (2016) 98874–98892.

[4] I.K.M. Yu, D.C.W. Tsang, Bioresour. Technol. 238 (2017) 716–732.

[5] E. Nikolla, Y. Román-Leshkov, M. Moliner, M.E. Davis, ACS Catal. 1 (2011) 408–410.

[6] M. Moliner, Y. Roman-Leshkov, M.E. Davis, Proc. Natl. Acad. Sci. 107 (2010) 6164–6168.

[7] C. Jiang, J. Zhu, B. Wang, L. Li, H. Zhong, Chinese J. Chem. Eng. 26 (2018) 1270–1277.

[8] C. Moreau, R. Durand, S. Razigade, J. Duhamet, P. Faugeras, P. Rivalier, R. Pierre, G. Avignon, Appl. Catal. A Gen. 145 (1996) 211–224.

[9] S. De, S. Dutta, B. Saha, Green Chem. 13 (2011) 2859–2868.

[10] J.N. Chheda, Y. Román-Leshkov, J.A. Dumesic, Green Chem. 9 (2007) 342–350.

[11] J.N. Chheda, J. a Dumesic, Science. 312 (2006) 1933.

[12] A. Dutta, D. Gupta, A.K. Patra, B. Saha, ChemSusChem. 7 (2014) 925–933.

[13] D. Prat, A. Wells, J. Hayler, H. Sneddon, C.R. McElroy, S. Abou-Shehada, P.J. Dunn, Green Chem. 18 (2015) 288–296.

[14] C. García-Sancho, I. Fúnez-Núñez, R. Moreno-Tost, J. Santamaría-González, E. Pérez-Inestrosa, J.L.G. Fierro, P. Maireles-Torres, Appl. Catal. B Environ. 206 (2017) 617–625.

[15] A. Pallagi, C. Dudás, Z. Csendes, P. Forgó, I. Pálinkó, P. Sipos, J. Mol. Struct. 993 (2011) 336–340.

[16] T. Zhang, R. Kumar, C.E. Wyman, RSC Adv. 3 (2013) 9809–9819.

[17] X. Zhang, P. Murria, Y. Jiang, W. Xiao, H.I. Kenttämaa, M.M. Abu-Omar, N.S. Mosier, Green Chem. 18 (2016) 5219–5229.

[18] L. Hu, Z. Wu, J. Xu, Y. Sun, L. Lin, S. Liu, Chem. Eng. J. 244 (2014) 137–144.

[19] G. Sampath, K. Srinivasan, Appl. Catal. A Gen. 533 (2017) 75–80.

[20] M. Watanabe, Y. Aizawa, T. Iida, R. Nishimura, H. Inomata, Appl. Catal. A Gen. 295 (2005) 150–156.

[21] M. Watanabe, Y. Aizawa, T. Iida, T.M. Aida, C. Levy, K. Sue, H. Inomata, Carbohydr. Res. 340 (2005) 1925–1930.

[22] X. Qi, M. Watanabe, T.M. Aida, R.L. Smith, Catal. Commun. 9 (2008) 2244–2249.

[23] A. Chareonlimkun, V. Champreda, A. Shotipruk, N. Laosiripojana, Fuel. 89 (2010) 2873–2880.

[24] C. García-Sancho, I. Sádaba, R. Moreno-Tost, J. Mérida-Robles, J. Santamaría-González, M. López-Granados, P. Maireles-Torres, ChemSusChem. 6 (2013) 635–642.

[25] Y. Zhang, Q. Xiong, Y. Chen, M. Liu, P. Jin, Y. Yan, J. Pan, Ind. Eng. Chem. Res. 57 (2018) 1968–1979.

[26] C. García-Sancho, J.M. Rubio-Caballero, J.M. Mérida-Robles, R. Moreno-Tost, J. Santamaría-González, P. Maireles-Torres, Catal. Today. 234 (2014) 119–124.

[27] I. Jiménez-Morales, J. Santamaría-González, A. Jiménez-López, P. Maireles-Torres, Fuel. 118 (2014) 265–271.

[28] A. Corma, Chem. Rev. 97 (2002) 2373–2420.

[29] A. Taguchi, F. Schüth, Microporous Mesoporous Mater. 77 (2005) 1-45.

[30] D. Trong On, D. Desplantier-Giscard, C. Danumah, S. Kaliaguine, Appl. Catal. 222 (2001) 299-357.

[31] I. Jiménez-Morales, M. Moreno-Recio, J. Santamaría-González, Appl. Catal. B Environ. 164 (2015) 70–76.

[32] A. Mukherjee, M.J. Dumont, V. Raghavan, Biomass and Bioenergy. 72 (2015) 143–183.

[33] E. Rodríguez-Castellón, A. Jiménez-López, P. Maireles-Torres, D.J. Jones, J. Rozière, M. Trombetta, G. Busca, M. Lenarda, L. Storaro, J. Solid State Chem. 175 (2003) 159–169.

[34] X. Lai, D. Wang, N. Han, J. Du, J. Li, C. Xing, Y. Chen, X. Li, Chem. Mater. 22 (2010) 3033–3042.

[35] J. Hu, W. Shan, W. Zhang, Y. Zhang, Y. Tang, Microporous Mesoporous Mater. 129 (2010) 210–219.

[36] S. Gopinath, P.S.M. Kumar, K.A.Y. Arafath, K. V. Thiruvengadaravi, S. Sivanesan, P. Baskaralingam, Fuel. 203 (2017) 488–500.

[37] C. García-Sancho, R.M.A. Saboya, J.A. Cecilia, A. V. Sales, F.M.T. Luna, E. Rodríguez-Castellón, C.L. Cavalcante, Mol. Catal. 436 (2017) 267–275.

[38] D.J. Jones, J. Jiménez-Jiménez, A. Jiménez-López, P. Maireles-Torres, P. Olivera-Pastor, E. Rodriguez-Castellón, J. Rozière, Chem. Commun. 2 (1997) 431–432.

[39] J.A. Cecilia, E. Vilarrasa-García, C. García-Sancho, R.M.A. Saboya, D.C.S. Azevedo, C.L. Cavalcante, E. Rodríguez-Castellón, Int. J. Greenh. Gas Control. 52 (2016) 344–356.

[40] P. Wrigstedt, J. Keskiväli, T. Repo, RSC Adv. 6 (2016) 18973–18979.

[41] T.W. Kim, F. Kleitz, B. Paul, R. Ryoo, J. Am. Chem. Soc. 127 (2005) 7601–7610.

[42] P. Wrigstedt, J. Keskiväli, M. Leskelä, T. Repo, ChemCatChem. 7 (2015) 501–507.

[43] A. Ramanathan, B. Subramaniam, R. Maheswari, U. Hanefeld, Microporous Mesoporous Mater. 167 (2013) 207–212.

[44] C. García-Sancho, R. Moreno-Tost, J. Mérida-Robles, J. Santamaría-González, A. Jiménez-López, P. Maireles-Torres, Appl. Catal. A Gen. 433–434 (2012) 179–187.

[45] M. Thommes, K. Kaneko, A. V. Neimark, J.P. Olivier, F. Rodriguez-Reinoso, J. Rouquerol, K.S.W. Sing, Pure Appl. Chem. 87 (2015) 1051–1069.

[46] A. Galarneau, H. Cambon, F. Di Renzo, F. Fajula, Langmuir. 17 (2001) 8328–8335.

[47] A. Ramírez, B.L. Lopez, L. Sierra, J. Phys. Chem. B. 107 (2003) 9275–9280.

[48] I. Fúnez-Núñez, C. García-Sancho, J.A. Cecilia, R. Moreno-Tost, E. Pérez-Inestrosa, L. Serrano-Cantador, P. Maireles-Torres, Appl. Catal. A Gen. 585 (2019) 117188.

[49] J.M.R. Gallo, C. Bisio, G. Gatti, L. Marchese, H.O. Pastore, Langmuir. 26 (2010)

5791–5800.

[50] H. Atia, U. Armbruster, A. Martin, Appl. Catal. A Gen. 393 (2011) 331–339.

[51] H.J.M. Bosman, A.P. Pijpers, A.W.M.A. Jaspers, J. Catal. 161 (1996) 551–559.

[52] C. García-Sancho, J.A. Cecilia, A. Moreno-Ruiz, J.M. Mérida-Robles, J. Santamaría-González, R. Moreno-Tost, P. Maireles-Torres, Appl. Catal. B Environ. 179 (2015) 139–149.

[53] A. Ramanathan, M. Carmen Castro Villalobos, C. Kwakernaak, S. Telalovic, U. Hanefeld, Chem. - A Eur. J. 14 (2008) 961–972.

[54] F. Verpoort, G. De Doncker, A.R. Bossuyt, L. Fiermans, L. Verdonck, J. Electron Spectros. Relat. Phenomena. 73 (1995) 271–281.

[55] M.D. Gracia, A.M. Balu, J.M. Campelo, R. Luque, J.M. Marinas, A.A. Romero, Appl. Catal. A Gen. 371 (2009) 85–91.

[56] I. Agirrezabal-Telleria, I. Gandarias, P.L. Arias, Catal. Today. 234 (2014) 42–58.

[57] S.K. Tyrlik, D. Szerszen, M. Olejnik, W. Danikiewicz, Journal Molecular Catalysis A. 106 (1996) 223-233.

[58] G. Tsilomelekis, M.J. Orella, Z. Lin, Z. Cheng, W. Zheng, V. Nikolakis, D.G. Vlachos, Green Chem. 18 (2016) 1983–1993.

[59] M. Moreno-Recio, J. Santamaría-González, P. Maireles-Torres, Chem. Eng. J. 303 (2016) 22–30.

[60] Z. Cheng, J.L. Everhart, G. Tsilomelekis, V. Nikolakis, B. Saha, D.G. Vlachos, Green Chem. 20 (2018) 997–1006.

Table 1. Textural and acidic properties of Zr-X(y) catalysts

Sample	S_{BET} ($m^2 \cdot g^{-1}$)	V_P ($cm^3 \cdot g^{-1}$)	S^a ($m^2 \cdot g^{-1}$)	$V_P{}^a$ ($cm^3 \cdot g^{-1}$)	µmoles $NH_3 \cdot g_{cat}^{-1}$	µmoles $NH_3 \cdot m^{-2}$
KIT-6	911	1.2	1149	1.147	n.d.	n.d.
Zr-KIT(30)	825	1.313	1171	1.234	622	0.754
Zr-KIT(14)	747	1.328	1010	1.090	833	1.115
Zr-KIT(5)	701	0.540	697	0.606	817	1.165
Zr-HMS(5)	909	0.528	733	0.582	501	0.551
Zr-SBA-HT(5)	462	0.753	494	0.642	746	1.615
Zr-SBA(5)	749	0.346	744	0.525	676	0.902
Zr-MCM(5)	564	0.413	396	0.214	495	0.878

[a]: determined by MP method; n.d.: not detected

Table 2. XPS data of Zr-X(y) catalysts.

Catalyst	Binding Energy (eV)			Atomic ratio	
	O 1s	Si 2p	Zr $3d_{5/2}$	Si/Zr_{XPS}	Si/Zr_{bulk}
Zr-KIT(30)	532.4	103.8	182.9	29.1	30
Zr-KIT(14)	532.7	103.4	183.3	19.4	14
Zr-KIT(5)	530.8 (5.1%) 532.7 (94.9%)	103.3	183.2	12.1	5
Zr-HMS(5)	530.7 (7.8%) 532.8 (92.2%)	103.5	182.8	9.9	5
Zr-SBA-HT(5)	531.1 (4.5%) 532.9 (95.5%)	103.5	183.4	32.3	5
Zr-SBA(5)	530.7 (4.6%) 532.4 (95.4%)	103.1	182.9	20.8	5
Zr-MCM(5)	530.8 (4.7%) 533.0 (95.3%)	103.7	182.8	13.4	5

List of captions.

Figure 1. XRD patterns at low-angle region of A) Zr-KIT(y) catalysts.

Figure 2. TEM micrographs of (A) Zr-KIT(5) (B) Zr-HMS(5) (C) Zr-MCM(5) (D) Zr-SBA(5) (E) Zr-SBA-HT(5).

Figure 3. N_2 adsorption-desorption isotherms of A) Zr-KIT(y) and B) Zr-X(5) catalysts.

Figure 4. Pore size distribution curves determined by DFT method for A) Zr-KIT(y) and B) Zr-X(5) catalysts and evaluated by MP method for C) Zr-KIT(y) and D) Zr-X(5) catalysts.

Figure 5. FTIR of adsorbed pyridine spectra of A) Zr-KIT(5), B) Zr-MCM(5), C) Zr-SBA(5), D) Zr-SBA-HT(5), E) Zr-HMS(5).

Figure 6. A) Effect of $CaCl_2$ addition ($0.650 g \cdot g_{aqueous\ solution}^{-1}$) after 60min and B) influence of reaction time for Zr-KIT(y) on glucose conversion and HMF yield (175ºC, H_2O:MIBK=1.5mL:3.5mL and a glucose:catalyst ratio of 3).

Figure 7. Influence of the reaction time on glucose conversion, fructose and HMF yields for Zr-X(5) catalysts (175ºC, H_2O:MIBK=1.5mL:3.5mL, 0.65 g $CaCl_2 \cdot g_{aqueous\ solution}^{-1}$ and a glucose:catalyst ratio of 3).

Figure 8. Glucose conversion (squares) and HMF yield (circles) as function of A) surface Si/Zr molar ratio determined by XPS and B) surface Zr atoms$\cdot nm^{-2}$ (175ºC, 20 minutes H_2O:MIBK=1.5mL:3.5mL, 0.65 g $CaCl_2 \cdot g_{aqueous\ solution}^{-1}$ and a glucose:catalyst ratio of 3).

Figure 9. TG profiles of fresh catalysts and spent catalyst after 90 min at 175 ºC and 60 min at 150 ºC with/without washing with water or water/ketone.

Figure 10. Influence of the presence of pyridine on the glucose conversion and HMF and fructose selectivity (175ºC, 60 minutes and 5 mL of H_2O).

Figure 11. Effect of reaction temperature as function of reaction time at 150 ºC and 175 ºC for Zr-HMS(5) and comparison with non-catalytic process at 150 ºC (H_2O:MIBK=1.5mL:3.5mL, 0.65 g $CaCl_2 \cdot g_{aqueous\ solution}^{-1}$ and a glucose:catalyst ratio of 3).

Figure 12. Glucose conversion, HMF yield and fructose yield (A) and TON values (B) as function of glucose:catalyst weight ratio for Zr-HMS(5) (H_2O:MIBK=1.5mL:3.5mL, 0.15 g of glucose, 0.65 g $CaCl_2 \cdot g_{aqueous\ solution}^{-1}$, 150ºC and 3 hours).

Figure 13. Reuse of Zr-HMS(5) (150ºC, 60 minutes H_2O:MIBK=1.5mL:3.5mL, 0.65 g $CaCl_2 \cdot g_{aqueous\ solution}^{-1}$ and a glucose:catalyst ratio of 1).

Figure 14. Catalytic behaviour of Zr-HMS(5) for HMF production by using different disacharides and polysacharides as raw materials (175ºC, 60 minutes H_2O:MIBK=1.5mL:3.5mL, 0.65 g $CaCl_2 \cdot g_{aqueous\ solution}^{-1}$ and a glucose:catalyst ratio of 3).

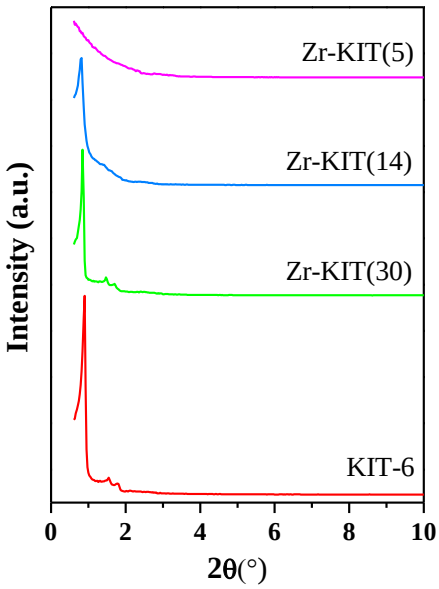

Figure 1.

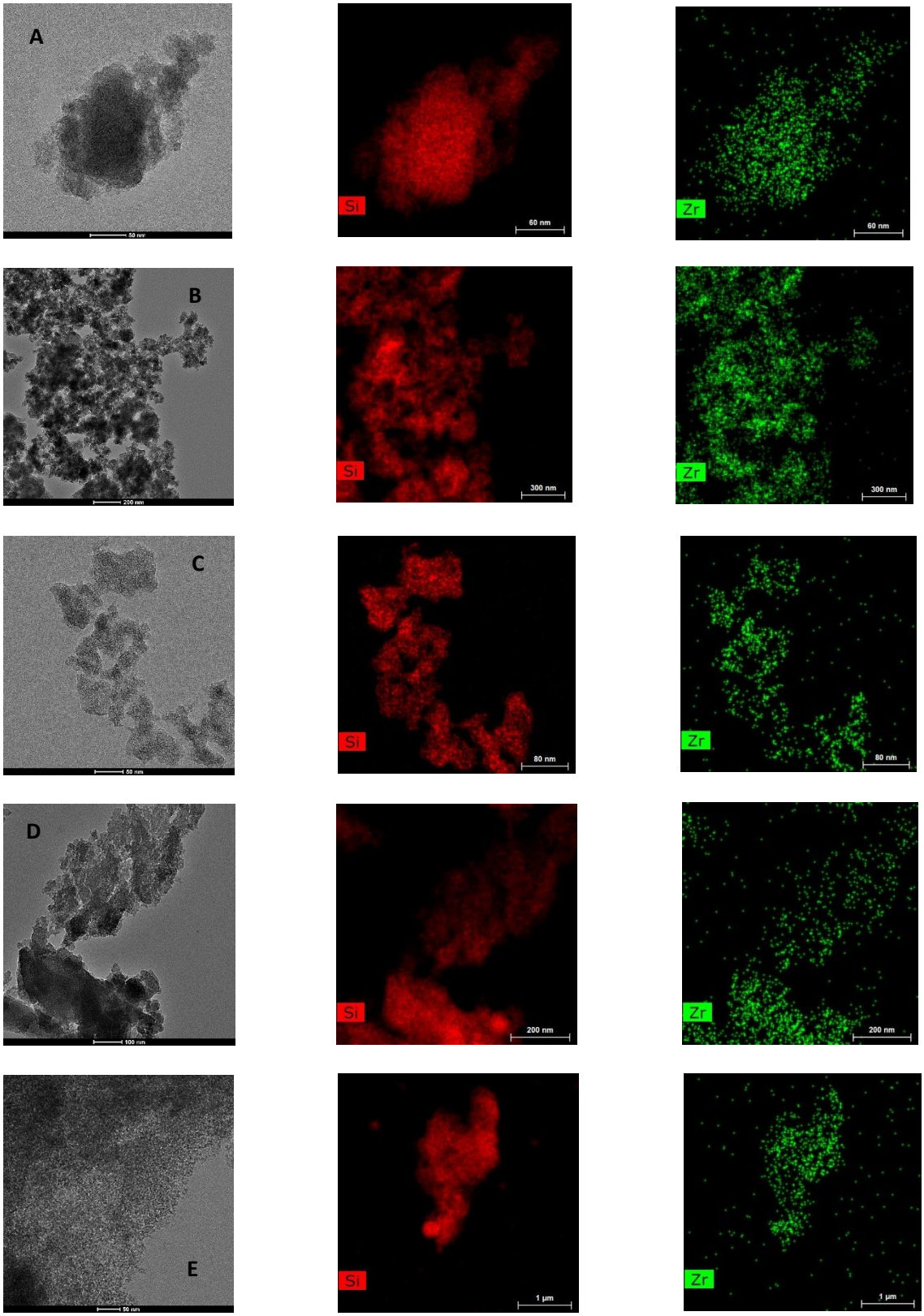
A
Si
60 nm
Zr
60 nm
B
Si
300 nm
Zr
300 nm
C
Si
80 nm
Zr
80 nm
D
Si
200 nm
Zr
200 nm
E
Si
1 µm
Zr
1 µm

Figure 2

A) **B)**

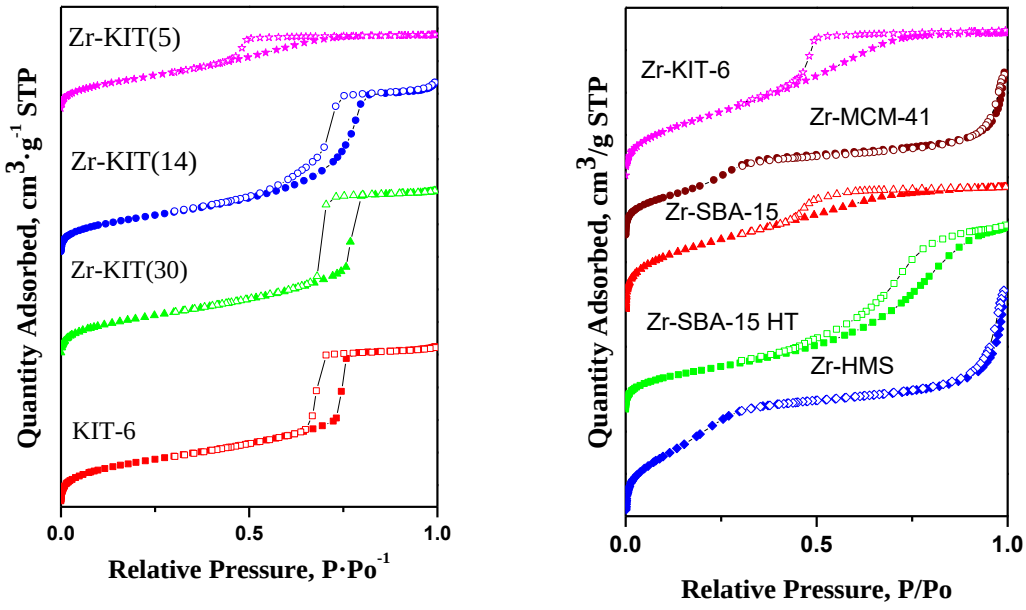

Figure 3

A) **B)**

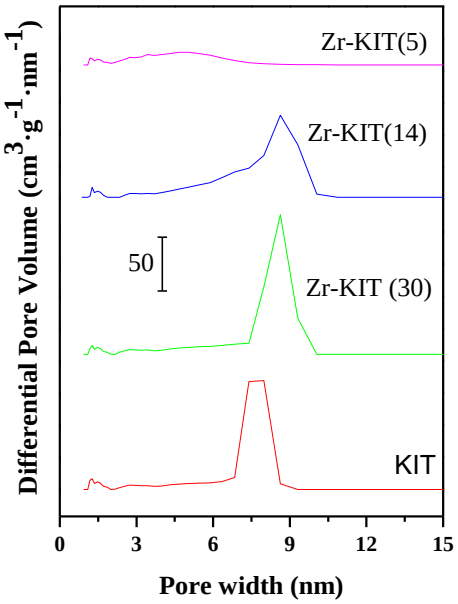
Zr-KIT(5)
Zr-KIT(14)
50
Zr-KIT (30)
KIT
Differential Pore Volume (cm3·g-1·nm-1)
0 3 6 9 12 15
Pore width (nm)

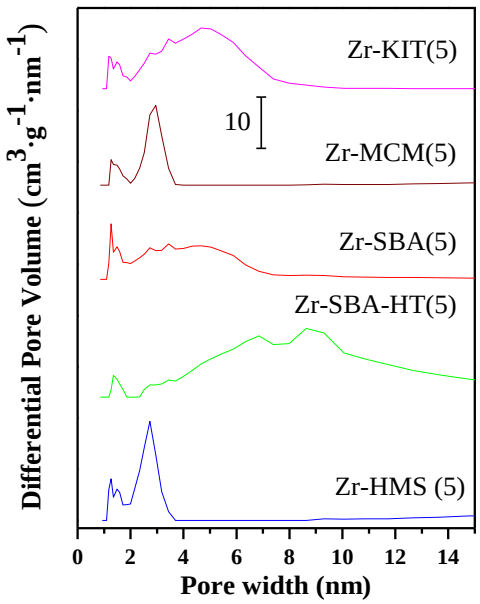
Zr-KIT(5)
10
Zr-MCM(5)
Zr-SBA(5)
Zr-SBA-HT(5)
Zr-HMS (5)
Differential Pore Volume (cm3·g-1·nm-1)
0 2 4 6 8 10 12 14
Pore width (nm)

C) **D)**

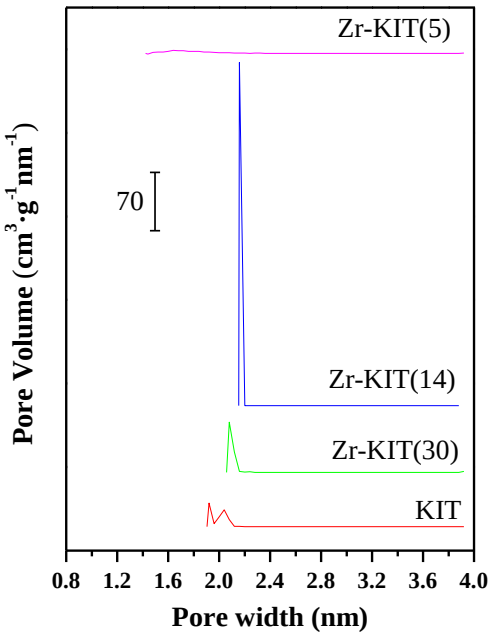
Zr-KIT(5)
70
Zr-KIT(14)
Zr-KIT(30)
KIT
Pore Volume (cm3·g-1nm-1)
0.8 1.2 1.6 2.0 2.4 2.8 3.2 3.6 4.0
Pore width (nm)

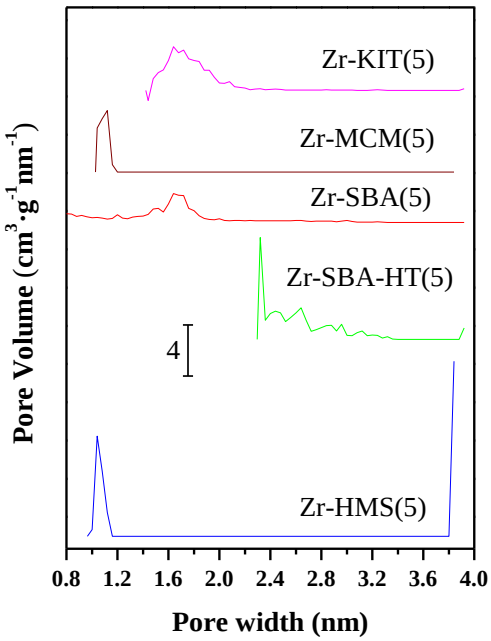
Zr-KIT(5)
Zr-MCM(5)
Zr-SBA(5)
Zr-SBA-HT(5)
4
Zr-HMS(5)
Pore Volume (cm3·g-1nm-1)
0.8 1.2 1.6 2.0 2.4 2.8 3.2 3.6 4.0
Pore width (nm)

Figure 4

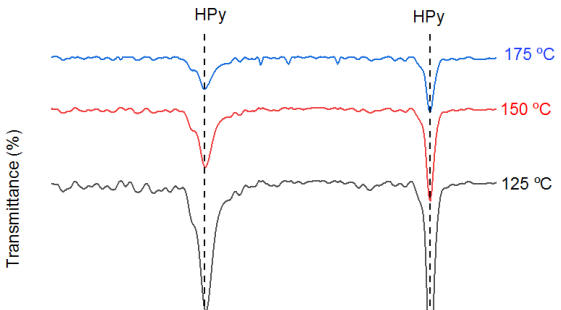
HPy
HPy
175 °C
150 °C
125 °C
Transmittance (%)

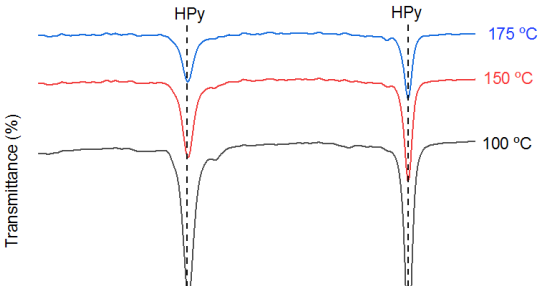
HPy
HPy
175 °C
150 °C
100 °C
Transmittance (%)

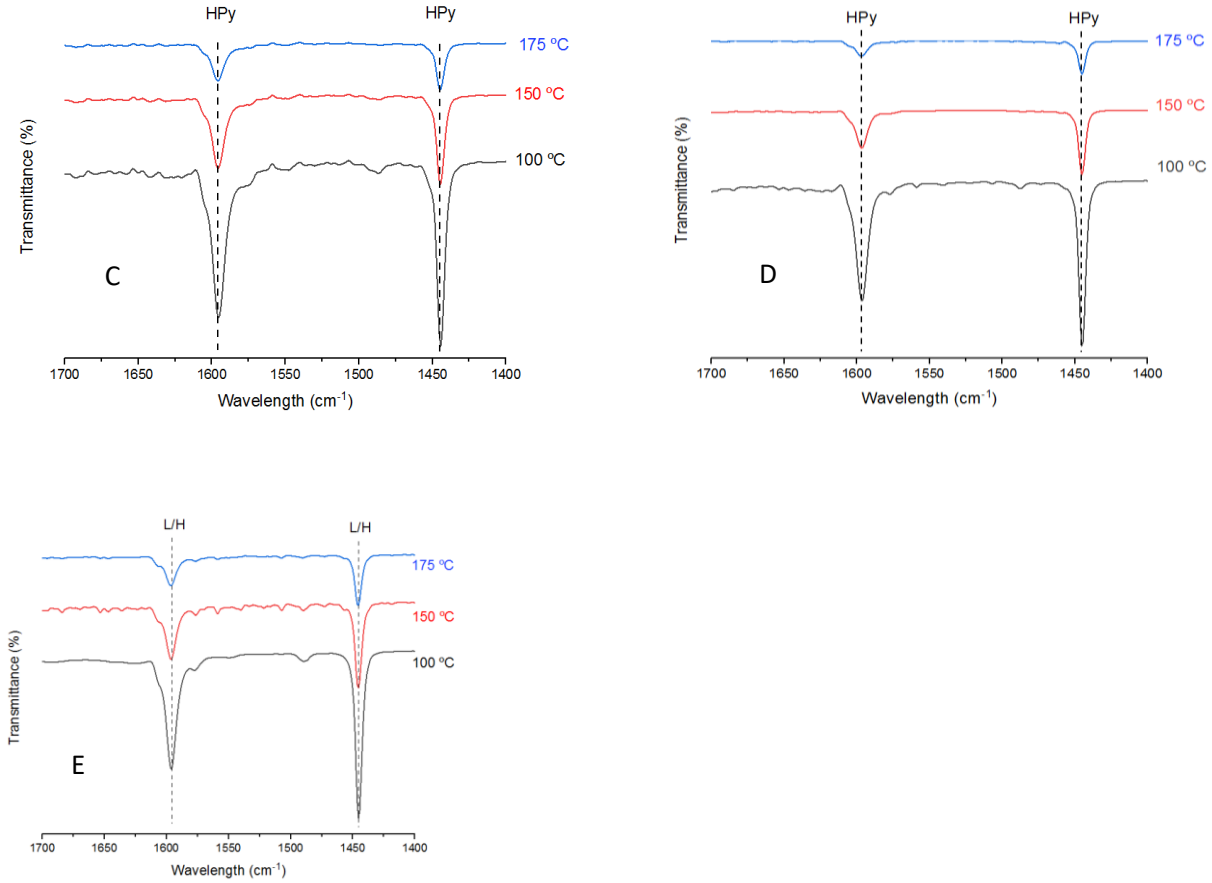
A
B
HPy
HPy
175 ºC
150 ºC
100 ºC
Transmittance (%)
C
Wavelength (cm-1)
1700
1650
1600
1550
1500
1450
1400
D
L/H
E

Figure 5

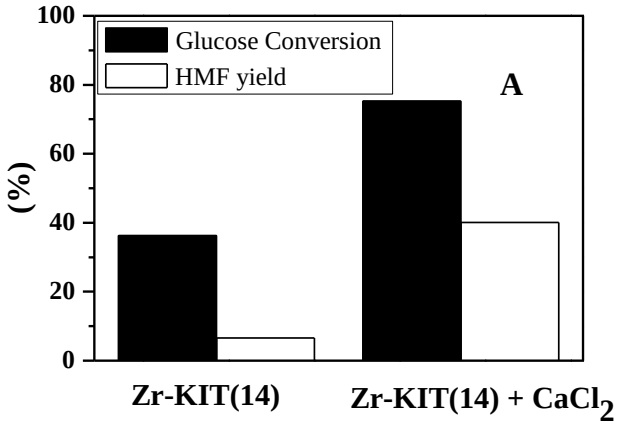
100
80
60
40
20
0
(%)
Glucose Conversion
HMF yield
A
Zr-KIT(14)
Zr-KIT(14) + CaCl2

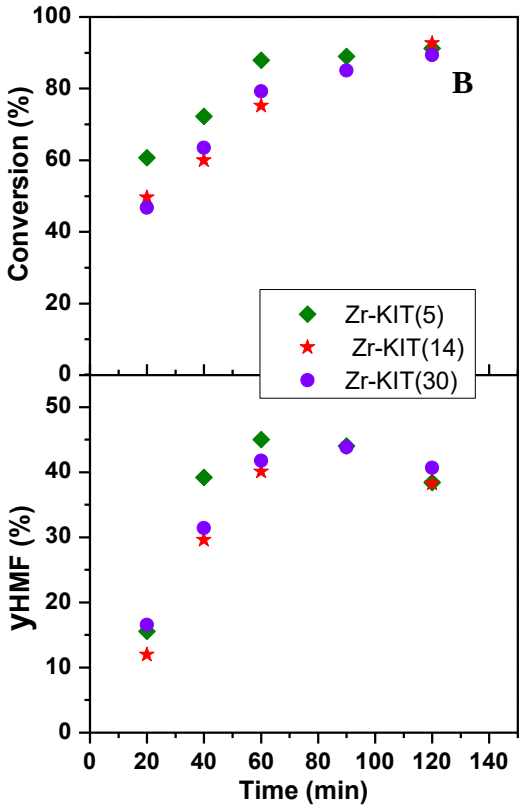
Conversion (%)
yHMF (%)
B
Zr-KIT(5)
Zr-KIT(14)
Zr-KIT(30)
Time (min)
0
20
40
60
80
100
120
140

Figure 6

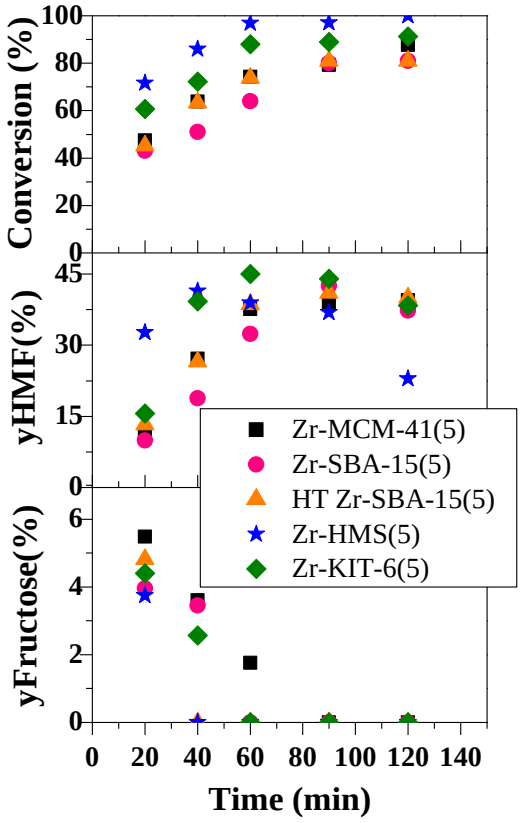
Conversion (%)
yHMF(%)
yFructose(%)
Time (min)
Zr-MCM-41(5)
Zr-SBA-15(5)
HT Zr-SBA-15(5)
Zr-HMS(5)
Zr-KIT-6(5)

Figure 7

A)

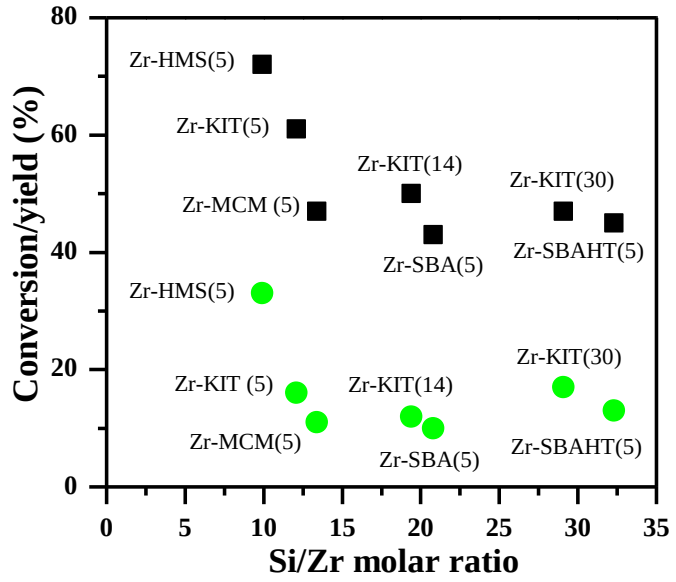
Conversion/yield (%)
Si/Zr molar ratio
0
20
40
60
80
0
5
10
15
20
25
30
35
Zr-HMS(5)
Zr-KIT(5)
Zr-KIT(14)
Zr-KIT(30)
Zr-MCM (5)
Zr-SBA(5)
Zr-SBAHT(5)
Zr-HMS(5)
Zr-KIT (5)
Zr-KIT(14)
Zr-KIT(30)
Zr-MCM(5)
Zr-SBA(5)
Zr-SBAHT(5)

B)

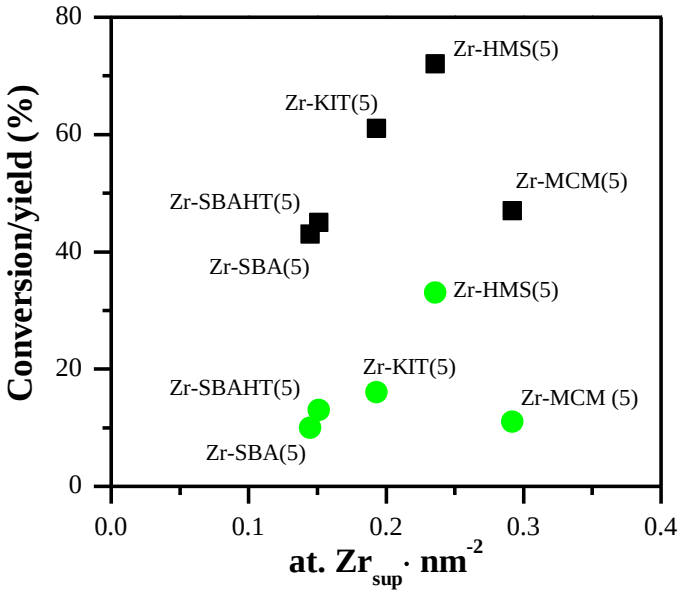
Conversion/yield (%)
at. Zr$_{sup}$ · nm^{-2}
0
20
40
60
80
0.0
0.1
0.2
0.3
0.4
Zr-HMS(5)
Zr-KIT(5)
Zr-MCM(5)
Zr-SBAHT(5)
Zr-SBA(5)
Zr-HMS(5)
Zr-KIT(5)
Zr-SBAHT(5)
Zr-MCM (5)
Zr-SBA(5)

Figure 8

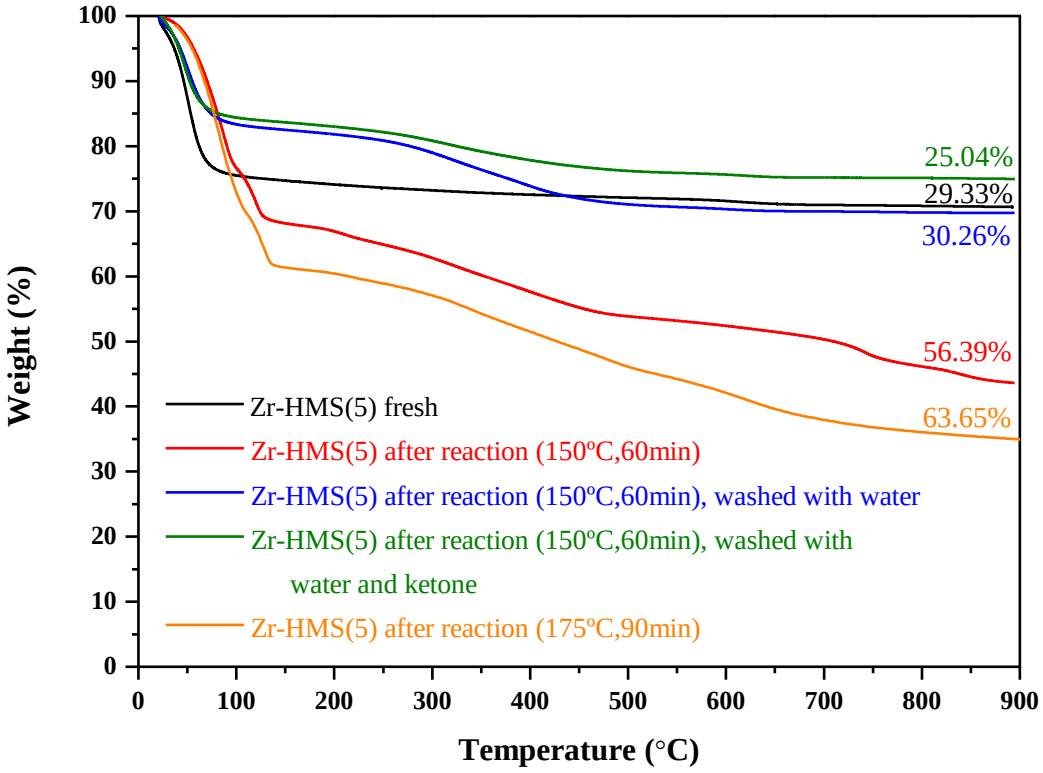
Weight (%)
Temperature (°C)
Zr-HMS(5) fresh
Zr-HMS(5) after reaction (150ºC,60min)
Zr-HMS(5) after reaction (150ºC,60min), washed with water
Zr-HMS(5) after reaction (150ºC,60min), washed with water and ketone
Zr-HMS(5) after reaction (175ºC,90min)
25.04%
29.33%
30.26%
56.39%
63.65%

Figure 9

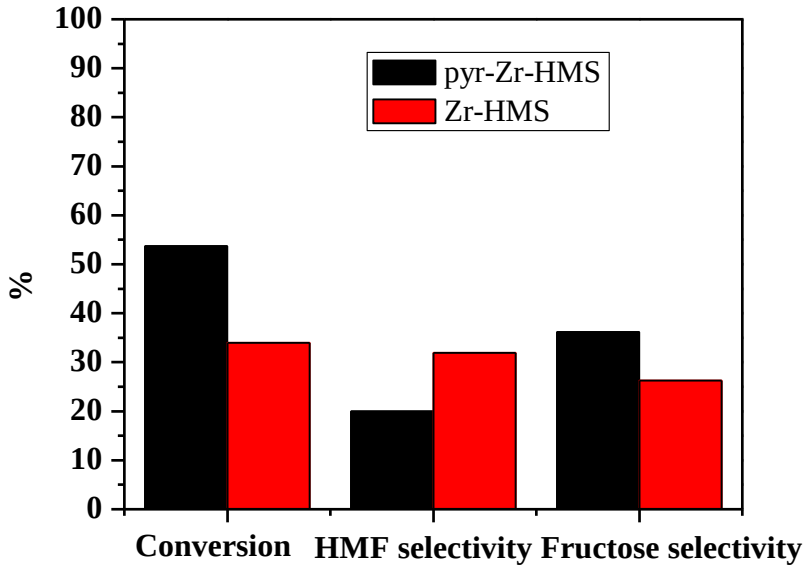
100
90
80
70
60
50
40
30
20
10
0
%
pyr-Zr-HMS
Zr-HMS
Conversion
HMF selectivity
Fructose selectivity

Figure 10

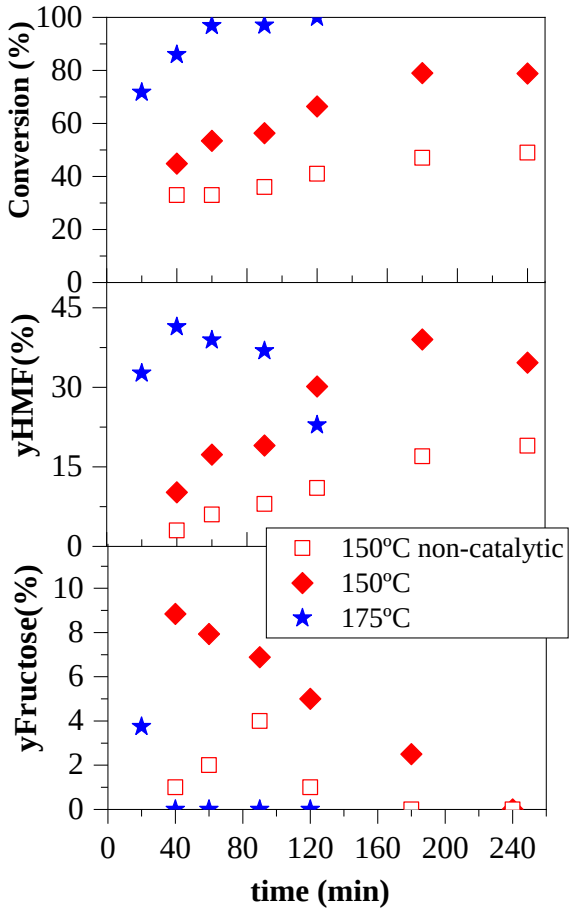
Conversion (%)
yHMF(%)
yFructose(%)
time (min)
150ºC non-catalytic
150ºC
175ºC

Figure 11

A)

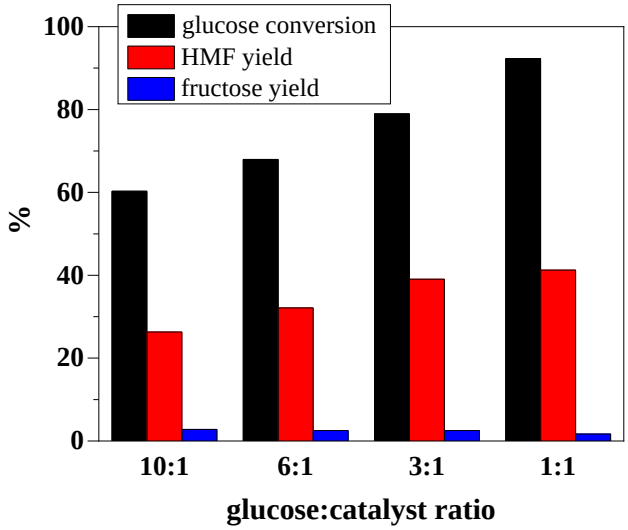
glucose conversion
HMF yield
fructose yield
100
80
60
40
20
0
%
10:1
6:1
3:1
1:1
glucose:catalyst ratio

B)

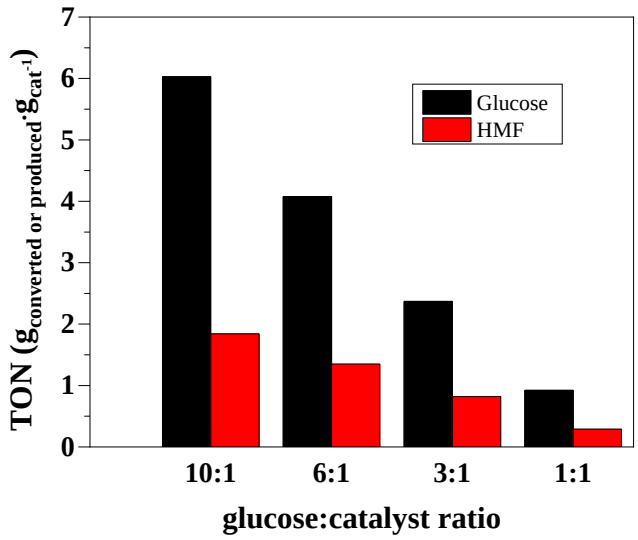
Glucose
HMF
7
6
5
4
3
2
1
0
TON (gconverted or produced·gcat-1)
10:1
6:1
3:1
1:1
glucose:catalyst ratio

Figure 12

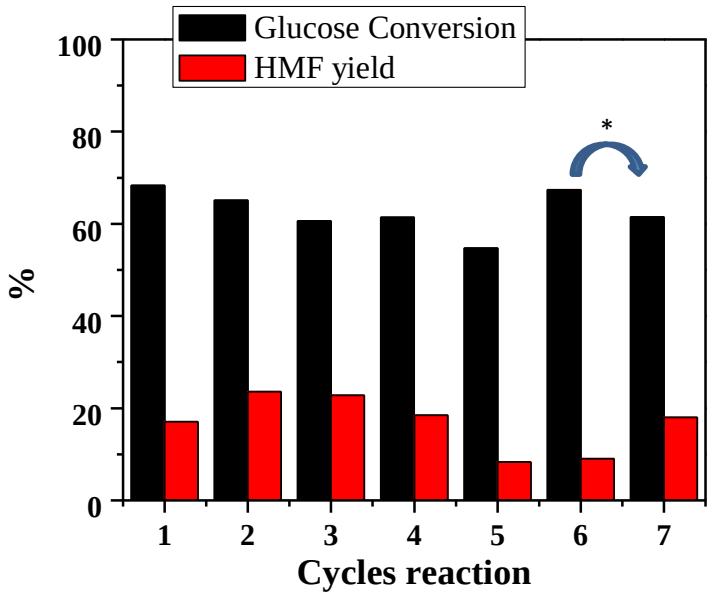
Glucose Conversion
HMF yield
100
80
60
40
20
0
%
1
2
3
4
5
6
7
*
Cycles reaction

Figure 13

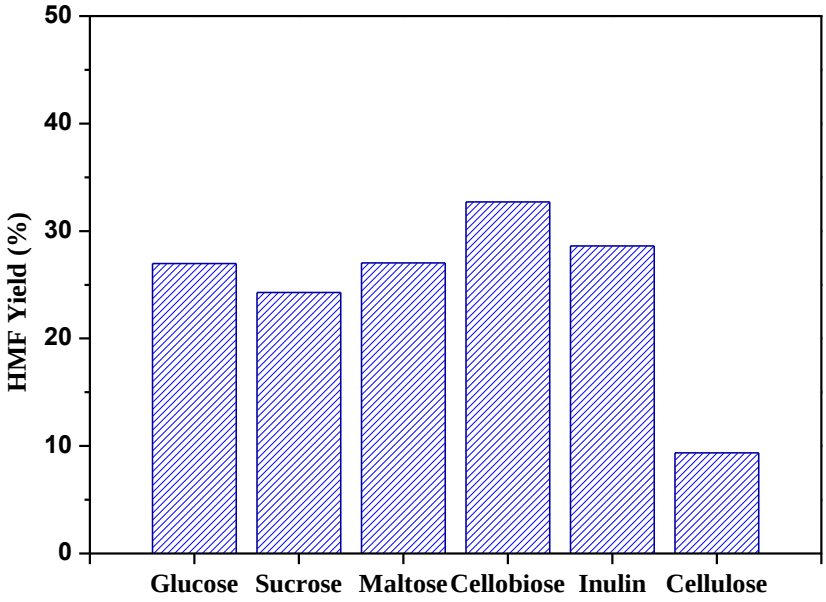
HMF Yield (%)
0
10
20
30
40
50
Glucose
Sucrose
Maltose
Cellobiose
Inulin
Cellulose

Figure 14